NASA TECHNICAL NOTE

NASA TN D-2871

FREE-FLIGHT MEASUREMENTS OF STAGNATION-POINT CONVECTIVE HEAT TRANSFER AT VELOCITIES TO 41,000 FT/SEC

by Dale L. Compton and David M. Cooper

Ames Research Center

Moffett Field, Calif.

NATIONAL AERONAUTICS AND SPACE ADMINISTRATION • WASHINGTON, D. C. • JUNE 1965

NASA TN D-2871

FREE-FLIGHT MEASUREMENTS OF STAGNATION-POINT CONVECTIVE HEAT TRANSFER AT VELOCITIES TO 41,000 FT/SEC

By Dale L. Compton and David M. Cooper

Ames Research Center
Moffett Field, Calif.

NATIONAL AERONAUTICS AND SPACE ADMINISTRATION

For sale by the Clearinghouse for Federal Scientific and Technical Information
Springfield, Virginia 22151 – Price $2.00

FREE-FLIGHT MEASUREMENTS OF STAGNATION-POINT CONVECTIVE HEAT TRANSFER AT VELOCITIES TO 41,000 FT/SEC

By Dale L. Compton and David M. Cooper
Ames Research Center

26597

SUMMARY

26597

Measurements of stagnation-point convective heat-transfer rates in air, at velocities to 41,000 ft/sec, are presented. A new technique was developed at the Ames Research Center to make these measurements. In this technique, 1/4-inch-diameter aluminum hemispheres are gun launched into the prototype of the Ames hypervelocity free-flight facility at a velocity of 24,000 ft/sec into still air, and at combined velocities of 36,000 and 41,000 ft/sec into the countercurrent airstream. At some point on its flight path the model begins to melt, and molten aluminum streams from the model surface into the wake, where it can be seen in spark shadowgraphs. The stagnation-point heating rate is then deduced by computing the heating rate required to produce melting at the observed time. The low-speed tests at 24,000 ft/sec served as calibration tests for the technique and showed its workability.

To study the possible effects of model material on the convective heating rate, several of the aluminum models were plated with a 0.0005-inch-thick nickel shell. These models were also subjected to calibration tests and then used for measuring convective heating rate at a velocity of 36,000 ft/sec.

The heating rates measured from all of the tests agree reasonably well with each other and with the majority of shock-tube data, and support theories which predict that ionization effects on convective heating rates in air will be small. No differences in heating rate were found for the two model surface materials tested.

author

INTRODUCTION

Significant numbers of ionized atoms are present in the shock layers on vehicles entering the earth's atmosphere at superorbital speeds. Several investigations, both theoretical and experimental, have been undertaken to determine whether this ionization has an important effect on convective heating. The results of the theoretical studies were originally in wide disagreement. However, theoreticians now generally agree that, for flight conditions studied to date, ionization results in only minor changes to the convective heating. All experimental data reported thus far for this speed range, with the exception of the results from the present tests, have been obtained with stationary models in shock tubes, and experimental disagreement exists among various sets of shock-tube data. Data taken with an independent technique are therefore of considerable value. One such technique, developed at the Ames Research Center, uses the time of onset of melting on small free-flying models

as a measure of the stagnation-point convective heating rate. It is the purpose of the present paper to describe this technique in detail, to report the data obtained, and to make a partial evaluation of the effect of surface material on convective heating.

SYMBOLS

a	thermal diffusivity of model material
A_c	maximum cross-sectional area
b,d	grouping defined by equations (9)
C	constant of proportionality
C_D	total drag coefficient
h	enthalpy
k	grouping defined by equations (A3)
K	thermal conductivity of model material
l	thickness of material 1 (appendix A)
m	model mass
N_R	Reynolds number, $\frac{V_\infty \rho_s R}{\mu_s}$
P	pressure
$\dot{q}$	heat-transfer rate
R	radius of curvature of model face
S	shear stress gradient
t	time
T	temperature
V	velocity
x	distance along the flight path
y	distance into the model from the stagnation point, normal to the surface
α	grouping defined by equations (A3)

β . grouping in equation (8)

γ factor of proportionality in equation (6)

μ viscosity

ρ air density

ρ_o standard atmospheric density

σ grouping defined by equations (A3)

τ dummy variable of integration

Subscripts

i conditions prior to launch

L launch conditions

s conditions immediately behind shock

st stagnation conditions

w wall (model surface) conditions

∞ free-stream conditions

1 material 1

2 material 2

EXPERIMENTS

Melting Onset Technique

This technique uses the time of onset of melting on small aluminum models as a measure of the stagnation-point heating rate. A sabot-held aluminum hemisphere is gun launched at high velocity either into still air in a ballistic range or into an oncoming airstream in a free-flight wind tunnel. Heating experienced by the model as it decelerates raises its temperature and at some point along the flight path the surface of the model begins to melt. Melting occurs first in the stagnation region, where the heating rate is highest. Since the viscosity of molten aluminum is low, aluminum flows off the model surface and into the wake. This liquid aluminum runoff produces a partially opaque screen which is visible in the wake region on spark shadowgraphs. If the free-stream density and model size are adjusted correctly, melting can be made to begin while the model is flying through the instrumented test section of the range; thus the time at which melting first occurs

can be determined from successive shadowgraphs. With the time of melting onset known, the stagnation-point heating rate can be determined by solving the heat-conduction equation for the model interior. This technique is described in detail in the following sections.

Test Equipment

Models were launched from a light-gas gun into the prototype of the Ames hypervelocity free-flight facility, which may be operated either as a ballistic range or as a free-flight wind tunnel. A schematic view of the facility is shown as figure 1. The model launcher used for these tests was a caliber 0.50 deformable-piston, light-gas gun. Models fly through a test section beginning 15 feet from the gun muzzle, instrumented with 11 spark shadowgraph stations spaced at 4-foot intervals along its length.[1] Model time of flight between stations is recorded on electronic chronographs. The time-distance and angle-of-attack histories of the model are extracted from the shadowgraph pictures and chronograph records. An enlarged view of part of the test section is shown in the inset of figure 1.

When this facility is used as a free-flight wind tunnel, the airstream is supplied from a 40-foot-long, 6-1/4-inch-diameter shock tube coupled to a combustion chamber of like dimensions. The energy for driving the shock tube is supplied by the constant volume combustion of H_2 and O_2 diluted with He or He and N_2. The shock-tube diaphragm is punctured shortly after the combustion process has reached peak temperature and pressure. The initial pressure ratio between the driver and driven gas, adjusted to tailor the reflected shock wave at the interface, produces a stagnation region of high-temperature, high-pressure air. A second diaphragm separating the stagnation region of the shock tube from the test section breaks spontaneously soon after the incident shock wave reflects from it, allowing flow to begin in the wind tunnel. The pressure in the test section is set prior to the run at such a level that wind-tunnel starting transients are minimized. The contoured nozzle provides a nominal Mach number 7 airstream which exhausts into a large vacuum tank at the end of the test section. A more complete description may be found in reference 1.

Models and Sabots

The models were 1/4-inch-diameter 7075 T6 aluminum hemispheres. This model was chosen because it is relatively easy to launch and because the stagnation-point heating rate is insensitive to small angle of attack.

A sketch of a model and sabot is shown in figure 2. The sabot, in addition to its usual functions of supporting the model during launch and providing

[1] A recent innovation to this system has been to adapt some of the shadowgraphs for use with Kerr-cell shutters to shorten exposure times from about 0.2 microsecond to 0.03 microsecond. The increase in model image sharpness is striking (see fig. 6).

a seal between the model and launch barrel, was designed to fully enclose the model to reduce heating to the model from three sources - barrel friction, compressed gas in front of the sabot, and driver gas behind the sabot. To further protect the model from heating from the hot gun gases, a polyethylene gas seal was placed behind the sabot and several pieces of 0.001-inch-thick mylar were placed against the base of the model. Although no tests were made to determine how effective this particular design was in protecting the model from extraneous heating, a similar model and sabot configuration (ref. 2) was extremely successful.

The total weight of the model and sabot was 1.3 grams. The maximum launch velocity attained was 26,960 ft/sec and velocities greater than 26,000 ft/sec were attained routinely.

To study the possible effects of gage material on convective heating, the surfaces of several aluminum models were nickel-electroplated. The thickness of the nickel coating was 0.0005 inch, thick enough to assure a coherent nickel surface (shown by examination of the model under a microscope) and thin enough that for purposes of solving the heat-conduction equation for the interior of the model the nickel coat could be neglected (calculations leading to this conclusion are presented in appendix A). Therefore, with respect to convective heat transfer, these nickel-plated models had the surface properties (and therefore the catalytic efficiency with respect to surface recombination) of nickel, and with respect to conduction within the model, they had primarily the bulk properties of aluminum. Thus the heating-rate data taken using these nickel-plated models do not depend on the exact numerical values of the thermal properties of nickel.

Test Conditions

The results of tests at three different velocities are described in this paper. The nominal test conditions are summarized in the table below.

Test velocity, ft/sec	24,000	36,000	41,000
Model velocity, ft/sec	24,000	24,000	26,500
Airstream velocity, ft/sec	0	12,000	14,500
Airstream reservoir press, atm	---	138	160
ρ_∞, slugs/ft^3	1.6×10^{-4} - 2.9×10^{-4}	1.5×10^{-5}	0.6×10^{-5}
P_∞, atm	0.066 - 0.120	0.021	0.011
P_{st}, atm	43 - 76	8.8	4.6
Reynolds number, N_R	1.48×10^5 - 2.59×10^5	1.54×10^4	7.73×10^3

It is of interest to compare these conditions with the conditions attained in shock-tube tests on fixed models at comparable total enthalpy levels. If the shock-tube test conditions in the following table are compared with those in the table above we see that, at the higher velocity conditions where ionization is appreciable, the stagnation conditions are similar. Simulated

Reynolds numbers in shock-tube tests are generally higher than in the present tests, partly because of larger shock-tube models. The Reynolds numbers given in the table below are based upon a 1/4-inch model nose radius.

Simulated velocity, ft/sec	24,000	36,000	41,000
Stagnation enthalpy, Btu/lb	11,640	26,040	33,740
Stagnation pressure, atm	4.6	3.6 - 14.4	4.6
Initial pressure, mm Hg	1.0	0.25 - 1.0	0.25
Reynolds number based on simulated velocity	3.77×10^4	1.43×10^4 - 4.87×10^4	1.55×10^4

DATA REDUCTION

Wind-Tunnel Data Reduction

To obtain heating-rate data, it is necessary to know the free-stream properties as a function of time along the flight trajectory. For the tests at 24,000 ft/sec, in which the models were fired into still air, the free-stream properties were determined from the measured pressure and temperature of the air in the tunnel immediately prior to the firing of each shot. For these tests the model, though decelerating, was flying into a constant density environment.

For the tests at 36,000 and 41,000 ft/sec, in which the models were fired into the supersonic airstream, a more complex situation existed. To reach the steady airstream, the model must fly across the vacuum tank (see fig. 1) where properties will be very poorly defined after the entry of flow from the wind tunnel. To avoid this difficulty, models were launched at such a time as to meet the airstream before it had begun to enter the vacuum tank. This procedure is illustrated in figure 3. It can be seen from this figure that the model must fly through three distinct regions: (1) the low-pressure (approximately 300 microns Hg) still air in the vacuum tank and in the entrance to the test section, (2) the wind-tunnel starting shock wave and the air initially in the tunnel which has been compressed by this starting shock wave, and (3) the desired test environment - the steady hypersonic airstream. The properties in each of these regions must be determined in order to assess the contribution of each to the total heating. In region 1 the air velocity is zero, and the temperature and pressure were measured prior to each test. Both the extent of and properties in region 2 were determined from calibration tests by measuring the tunnel pitot pressure and wall static pressure as functions of time. It was determined that the model flies through region 2 for a distance of about 6 to 8 feet. The measured speed of the starting shock wave and the measured properties in region 1 were used to calculate air velocity and density immediately behind the starting shock. The density and velocity were assumed to vary linearly between their values immediately behind the starting shock and their values in region 3. The effect of these assumptions on the test results will be considered in appendix B. The properties in region 3 were determined from measurements of (a) the pressure and temperature of the air in the shock

tube prior to the run, (b) the velocity of the initial shock wave in the shock tube, and (c) the pressure behind the reflected shock wave (the reservoir pressure driving the wind tunnel). From these measurements, the stagnation enthalpy for the wind-tunnel reservoir was calculated by applying the appropriate shock-tube equations. Wind-tunnel free-stream properties (the properties in region 3) were then determined from the static pressure measured at several points on the test section wall by assuming real-gas flow between the reservoir and the test section to be isentropic and in equilibrium.

For the 12,000 ft/sec airstream a probe mounted in the tunnel during calibration tests showed pitot pressures consistent with predictions based on the above measurements. For the 14,500 ft/sec airstream, the pitot probe showed somewhat lower (approximately 25 percent) pitot pressures than expected. The detailed reasons for these low pitot pressures are not presently understood, but they are probably due to energy losses in the tunnel. The effect of the resulting uncertainties in airstream properties on the heating rate is not severe, and will be considered in detail later.

Solutions to the Heat-Conduction Equation

In order to relate the melting onset time to the heat-transfer rate, it was necessary to solve the heat-conduction equation for the interior of the model. Calculations showed that for the short flight times being considered (approximately 2 msec) the appreciably heated layer within the model was thin (less than 10 percent of the model diameter), and that the one-dimensional form of the heat-conduction equation could be used. The boundary conditions are those for a semi-infinite slab, initially at uniform temperature, heated on its exposed surface with a time-dependent heating rate. The time dependence of the heating rate arises because of the changing free-stream conditions and velocity along the flight path.

Thus the equations to be solved are

$$\left.\begin{aligned} a\,\frac{\partial^2 T}{\partial y^2} &= \frac{\partial T}{\partial t} \qquad y > 0,\ t > 0 \\ T(y,0) &= T_i \\ -K\left(\frac{\partial T}{\partial y}\right)_{y=0} &= \dot{q}_{st} = f(t) \end{aligned}\right\} \tag{1}$$

The solution of this system is well known and can be written with the aid of Duhamel's integral (see, e.g., ref. 3, p. 76). The surface temperature is given by

$$(T_w - T_i) = \left(\frac{a}{\pi}\right)^{1/2} \frac{1}{K} \int_0^t \dot{q}_{st}(t - \tau)\, \frac{d\tau}{\tau^{1/2}} \tag{2}$$

which can be rewritten in a form more suitable for numerical integration as

$$T_w - T_i = 2\left(\frac{a}{\pi}\right)^{1/2} \frac{1}{K} \int_0^{\sqrt{t}} \dot{q}_{st}(t - \tau)\, d\sqrt{\tau} \tag{3}$$

where $\dot{q}$ is the heating rate, and the other quantities are defined in the Symbols. Thus if the heating rate is known as a function of time, the variation of surface temperature with time may be calculated.

At the low-velocity test condition (24,000 ft/sec) the model was flown into still air at constant density. One form of the trajectory equation which assumes constant drag coefficient and relates the velocity to the time of flight is

$$V = \frac{1}{\frac{\rho_\infty C_D A_c}{2m} t + \frac{1}{V_L}} \tag{4}$$

The stagnation-point heating rate for this test condition may be written (ref. 4)

$$\dot{q}_{st} = C\left(\frac{\rho_\infty}{R}\right)^{1/2} V_\infty^{3.15} \tag{5}$$

For constant density and model size, and for reasonably small changes in velocity, equation (5) may be approximated by

$$\dot{q}_{st} = \gamma V_\infty^{3} \tag{6}$$

If equations (2), (4), and (6) are combined, the equation for surface temperature may be written as

$$T_w - T_i = \frac{\dot{q}_{st_L}}{K V_L^3} \sqrt{\frac{a}{\pi}} \int_0^t \frac{d\tau}{\left[\frac{\rho_\infty C_D A_c}{2m}(t - \tau) + \frac{1}{V_L}\right]^3 \tau^{1/2}} \tag{7}$$

where $\dot{q}_{st_L}$ is the heating rate at the beginning of flight. This may be integrated to give

$$T_w - T_i = \frac{2\dot{q}_{st_L}}{K} \sqrt{\frac{at}{\pi}} \left\{ \frac{d^3}{8(bt + d)^2} \left[\frac{2(bt + d) + 3d}{d^2} + \frac{3}{2\sqrt{bt(bt + d)}} \ln \frac{\sqrt{bt + d} + \sqrt{bt}}{\sqrt{bt + d} - \sqrt{bt}} \right] \right\}$$

$$= \frac{2\dot{q}_{st_L}}{K} \beta \sqrt{\frac{at}{\pi}} \tag{8}$$

where

$$b = \frac{\rho_\infty C_D A_c}{2m}, \qquad d = \frac{1}{V_L} \tag{9}$$

and β is the term in braces. Equation (8) is a closed-form solution for the time dependence of the stagnation-point surface temperature of models fired into still air for short flights.

When the models are fired through the starting-transient flow into the countercurrent airstream, it is no longer possible to obtain a closed-form solution and equation (3) must be integrated numerically. The numerical integration of equation (3) was programmed for the IBM 7090 computer.

RESULTS AND DISCUSSION

Calibration Tests at 24,000 Ft/Sec

As a check on the validity of the technique for determining heating rate from melting onset, several tests were performed at conditions for which the effects of ionization should be small. As shown in the tabulated test conditions, the velocity chosen for these tests was nominally 24,000 ft/sec and free-stream density was varied from 1.6×10^{-4} to 2.9×10^{-4} slug/ft^3 (ρ/ρ_o = 0.066 to 0.120). The stagnation-point heating rate at these conditions is well known from theory (ref. 5) and from experiment (e.g., ref. 6) and the agreement between theory and experiment is good. The procedure was to examine all the shadowgraphs from each run to determine at which station melting was first observed. The inputs to equation (8) were then determined, with the initial heating rate computed from the theory of reference 5, and the stagnation-point surface temperature was computed as a function of time. (Averages of the thermal properties of 7075-T6 aluminum between room temperature and melting temperature were used in this calculation.) A typical set of data from one of these runs on an aluminum model is shown in figure 4. This figure shows successive shadowgraphs from the first six wind-tunnel stations. Nothing unusual is seen in the flow field behind the model until station 3, where slight wisps of aluminum appear as a partially opaque region at the rear corners of the model, proving that melting started before the model reached station 3 and probably after it passed station 2. As the model progresses downrange through the shadowgraph stations, more and more aluminum is visible at the shoulders and in the wake. Finally, the model is distorted by the loss of material. Shown on this figure is the elapsed time of flight to each station and the model surface temperature at each station computed from equation (8). It is significant that melting is first observed at almost exactly the time when the computed surface temperature reaches the melting temperature of 7075-T6 aluminum (1180° F). This provides a check on the validity of the technique and leads to confidence in its use at velocities where ionization is appreciable.

The results from all the aluminum model tests at 24,000 ft/sec are presented in figure 5. This is a correlation plot of the predicted value of $\beta\sqrt{t}$

from equation (8) for $\dot{q}_{st_L}$ given by the theory of reference 5 and for $T_w = 1180^\circ$ F versus the measured value for melting onset. The coordinate system allows differences in heating rate to appear linearly on the plot. The 45° line is the line of perfect correlation and it can be seen that the data lie extremely close to the line. It was not always possible to be as certain of the station in which melting first began as in the run shown on figure 4. Thus most of the data in figure 5 are presented as bars indicating the $\beta\sqrt{t}$ range from the time at which melting was first probable until it was first surely in evidence. In most cases, melting was probable in one station and certain in the next. However, in some runs, for example figure 4, melting was surely occurring in the first station in which anything unusual was observed; these data are represented on figure 5 by circles. The longest bars represent runs in which three stations were needed to determine the onset. These data scatter around the 45° line by +9 to -13 percent.

In addition to the time required for the model surface to come to melting temperature, time will be required both to melt a finite thickness of aluminum and for this molten aluminum to flow off the model and into the wake. Melting onset will not be observed until the total time for these three events has elapsed. The time required to melt a 0.001-inch-thick layer of aluminum at the stagnation point was computed from the known latent heat of fusion of aluminum and heating rate and was found to be slightly less than one-half the time required for the model to fly from one station to the next. This time corresponds to one-half the length of the shortest scatter bar of figure 5 and is therefore small compared to the time required for surface melting to begin.

The time required for molten aluminum to flow from the stagnation region to the shoulder of the model is difficult to estimate since it will depend on whether or not surface waves form in the molten aluminum. If surface waves form, as is probable, the dynamic pressure in the flow field will tend to sweep them off the surface rapidly - probably in a few model lengths of flight. If surface waves do not form, then surface shear stress will control the time required. A table of the ratio of the stagnation-point shear stress gradient for the various test conditions to the stagnation-point shear stress gradient for the 24,000 ft/sec lowest density tests is given below.

Velocity, ft/sec	$\frac{S}{S_{24,000}}$
24,000	1.0 - 1.33
36,000	.66
41,000	.52

The shear stress was varied over a 30-percent range in the tests at 24,000 ft/sec and no effect of changing shear stress could be discerned in the data. The shear stress is reduced by a factor of two for the higher speed tests.

The effects described above are present in both the calibration tests and the higher velocity tests. The heating rates and shear stresses do not change

greatly between test conditions, and this similarity implies that differences in these effects should remain insignificant in the higher velocity tests.

Additional calibration tests were performed on the nickel-plated models at similar test conditions. When these runs were analyzed, melting was not observed until the computed surface temperature was approximately 1260° F - that is, for comparable test conditions, the nickel-plated models flew farther downrange before the onset of melting. This difference is probably due to two effects. First, even though the nickel shell was thin, it absorbed a finite amount of heat, thus reducing the heating rate to the aluminum substrate. Computations (appendix A) showed that, over the trajectory, the heat-transfer rate to the aluminum should have been reduced by about 3 percent due to the presence of the shell. Second, at the time when the aluminum (melting temperature 1180° F) began to melt, the same computations showed that the nickel (melting temperature 2650° F) had not melted, and therefore retained some strength, apparently enough to contain the aluminum melt layer for a short time. A series of four shadowgraphs from one of the nickel-plated aluminum model tests, shown in figure 6, supports this contention. No melting is observed in stations 1 and 2, but in station 3 melting is definite and strong - as if the aluminum had suddenly burst the nickel shell. This figure may be contrasted with figure 4, where melting onset is not nearly so pronounced.

Tests at Higher Velocities

Since the calibration tests showed that the technique is usable, tests were conducted at velocities near 36,000 and 41,000 ft/sec. The tests at 36,000 ft/sec were conducted in a countercurrent airstream which had a nominal velocity of 12,000 ft/sec and the tests at 41,000 ft/sec in a nominal 14,500 ft/sec airstream. The melting onset time was determined in the same manner as in the lower speed tests. The calculation of heating rate from melting onset time is complicated, as noted earlier, by the sequence of free-stream conditions the model encounters. The technique of data reduction was to assume heating-rate histories along the trajectory, consistent with the variations of velocity and density encountered, and to compute the time-temperature history at the stagnation point from equation (3). The time at which the stagnation point was calculated to reach 1180° F (1260° F for the nickel-plated aluminum models) was then compared with the time at which melting was first observed. The heating-rate history was then adjusted until a self-consistent history was found for which the two times matched. Since, as will be shown in a later section, the major portion of the heating occurred in region 3 (see fig. 3), the calculated surface temperature is relatively insensitive to the choice of heating-rate equations in regions 1 and 2.

The data obtained in the higher speed tests are shown in figure 7, where the measured heating rates are plotted as a function of enthalpy difference across the boundary layer. Since a large amount of data is now available from several sources (refs. 7-11), no attempt has been made to show all the available data points individually. Instead, the band in which the majority of the shock-tube data fall is indicated as a crosshatched area on figure 7. It can

be seen that the present data fall within this band and agree reasonably well with the theory of Hoshizaki, which is also shown. That theory is representative of the several theoretical treatments for convective heating with ionization.

One set of experimental data (ref. 7) falls substantially higher - as much as a factor of 2 - than the crosshatched band in figure 7. These higher heating rates were measured in the shock-tube experiments of reference 7 on heat-transfer gages made of nickel, Hytemco (a nickel alloy), and gold, while similar measurements on platinum gages are within the crosshatched band. The data were taken both in air and in N_2-CO_2-A mixtures. The shock-tube data of reference 11 (in N_2-CO_2-A mixtures) do not show this difference between gage materials. It is clear from figure 7 that there was no difference in heating rate between the aluminum and nickel-plated aluminum models in the present tests.

CONCLUSIONS

From the results of these tests on 1/4-inch-diameter hemispheres it can be concluded that:

1. A new technique for measuring convective heat transfer has been developed which is sufficiently different from other methods of measurement to be considered independent.

2. The technique is reasonably accurate, yielding convective heat-transfer data that is defined within an estimated accuracy of ±20 percent at velocities to 41,000 ft/sec.

3. The data agree with the majority of the existing shock-tube data and with theories that predict the effects of ionization in air on the convective heat transfer will be minor.

4. The heat-transfer rates obtained using aluminum and nickel-plated aluminum models at comparable test conditions were essentially the same.

Ames Research Center
National Aeronautics and Space Administration
Moffett Field, Calif., March 3, 1965

APPENDIX A

DESIGN CALCULATIONS FOR NICKEL-PLATED MODELS

As mentioned in the text, the use of equation (3) for the nickel-plated aluminum models neglected the presence of the nickel shell. In order to design a model such that the thickness of the nickel shell would be thin enough to be neglected, the following computations were made.

Consider a composite solid of two different materials as sketched below.

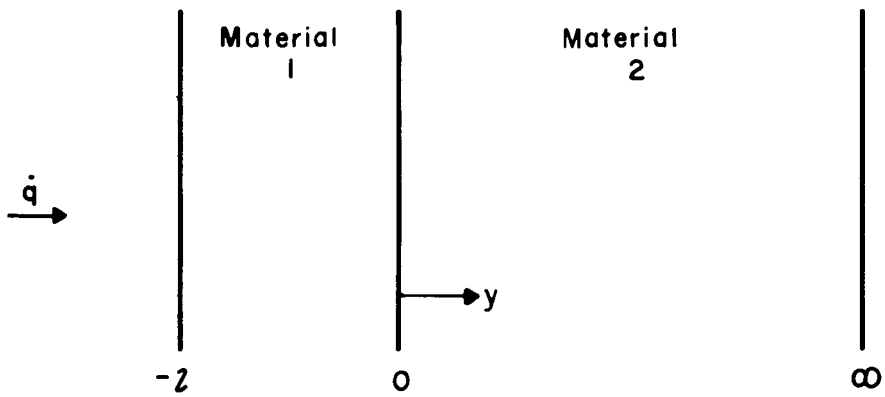

For a constant heat-transfer rate $\dot{q}$ at the surface $y = -l$, reference 3 (p. 322) gives the heat-transfer rate in the body as a function of time for the materials 1 and 2, respectively, as

$$\dot{q}_1 = \dot{q} \sum_{n=0}^{\infty} \alpha^n \left[\operatorname{erfc} \frac{(2n+1)l + y}{2\sqrt{a_1 t}} - \alpha \operatorname{erfc} \frac{(2n+1)l - y}{2\sqrt{a_1 t}} \right] \tag{A1}$$

$$\dot{q}_2 = \frac{2\dot{q}}{1+\sigma} \sum_{n=0}^{\infty} \alpha^n \operatorname{erfc} \frac{(2n+1)l + ky}{2\sqrt{a_1 t}} \tag{A2}$$

where

$$k = \sqrt{\frac{a_1}{a_2}}; \qquad \sigma = \left(\frac{K_2}{K_1} \sqrt{\frac{a_1}{a_2}} \right); \qquad \alpha = \frac{\sigma - 1}{\sigma + 1} \tag{A3}$$

Thus the heat input at $y = 0$ may be computed as a fraction of the heat input at $y = -l$ (for $\dot{q}_{y=-l}$ = constant). When the numerical values of the properties of nickel and aluminum and the time of flight were substituted into equation (A2), it was found that for a nickel shell of thickness 0.0005 inch, 97 percent of the heat transfer to the nickel reached the aluminum substrate. Furthermore, this fraction is insensitive to small changes in the nickel properties.

Since the success of the onset of ablation technique depends on the knowledge of the surface temperature, it is advisable to compute the ratio of the temperature at $y = 0$ for the composite model to the surface temperature of the pure aluminum model. With the relation

$$\dot{q} = -K \frac{\partial T}{\partial y} \tag{A4}$$

equations (A1) and (A2) may be integrated to give the temperature of the body as a function of time. Integration of these equations yields

$$T_1 - T_{y=o} = -\frac{2\dot{q}\sqrt{a_1 t}}{K_1} \sum_{n=o}^{\infty} \alpha^n \left\{ \left[(1 + \alpha)\ \text{ierfc}\ \frac{(2n + 1)l}{2\sqrt{a_1 t}} \right] \right.$$

$$\left. - \left[\text{ierfc}\ \frac{(2n + 1)l + y}{2\sqrt{a_1 t}} + \alpha\ \text{ierfc}\ \frac{(2n + 1)l - y}{2\sqrt{a_1 t}} \right] \right\} \tag{A5}$$

$$T_2 - T_i = \frac{2\dot{q}}{K_2(1 + \sigma)} \sum_{n=o}^{\infty} \alpha^n \left(\frac{2\sqrt{a_1 t}}{k} \right) \text{ierfc}\ \frac{(2n + 1)l + ky}{2\sqrt{a_1 t}} \tag{A6}$$

Specializing equation (3) of the text to the case for $\dot{q}_{st}$ = constant gives

$$T_w - T_i = \dot{q}_{st} \frac{2}{K} \sqrt{\frac{at}{\pi}} \tag{A7}$$

Substituting the appropriate numerical values into equations (A6) and (A7) shows that

$$\frac{T_{y=o} - T_i}{T_w - T_i} = 0.97$$

These computations show that if the presence of the nickel shell is neglected, when equation (3) is solved for the nickel-plated aluminum models, only small errors are introduced. These errors were compensated for by using the experimentally determined temperature for onset of melting on the nickel-plated aluminum models.

APPENDIX B

CONSIDERATIONS OF ERRORS AND OTHER FACTORS AFFECTING HEATING RATE

As with all heat-transfer measurement techniques, sources of error in the present technique are difficult to evaluate completely. If the calibration tests are considered alone, the deviation of the heating rate from the average is +9 and -13 percent. Part of this can be accounted for by the fact that the model is observed only at discrete times along the flight path and, therefore, melting onset is always observed sometime after it might first have occurred. On the average this possible systematic error is 6 percent. Therefore, other sources of error - for example, changes in heating during launch, changes in sabot separation from run to run and angle of attack - must account for the remainder of the deviation in the calibration tests.

For the tests conducted at 36,000 and 41,000 ft/sec an additional source of error is the uncertainty in the free-stream properties. The properties in region 2 (see fig. 3) are the least well determined, and it is desirable to estimate the effect of this uncertainty on the heating. A breakdown of the calculated heating distribution along the flight path for a typical run is given in the following table:

Region	Percent of heating
1	6
2	19
3	75

It can be inferred from this table that even relatively large errors in determining the properties in region 2 will not produce large errors in the deduced heat-transfer rates for region 3, since region 2 contributes a relatively small percentage of the total heating.

The sum of errors due to imperfect knowledge of the properties in region 3 can only be approximated. The scatter in the data taken using the countercurrent airstream, over and above the scatter in the calibration tests, can be taken as a measure of the random errors. The random scatter in the data is about ±16 percent for both the high-velocity test conditions, which indicates about ±5 percent additional random uncertainty. Systematic errors are possible. Total velocity and free-stream density both influence the heating rate. Fortunately, the velocity of the model relative to the tunnel (about 65 percent of the total velocity) is very well known. Therefore, even though the heating rate depends on V^3, a 10-percent error in airstream velocity in the tunnel leads to only an 11-percent error in heating rate. The heating rate depends on the square root of the free-stream density, so that a 10-percent error in free-stream density leads to a 5-percent error in heating rate. Whether errors of this order exist in the tunnel density and velocity is not known at the present time; however, they are sufficient to change the measured pitot pressure by 25 percent. When all the factors are weighed, an estimate of the accuracy of the measurements is ±20 percent. In general,

therefore, the accuracy of the technique can be considered acceptable, but not extraordinary. Its principal virtue is that it is different from other techniques and offers an independent method for obtaining experimental data.

The low Reynolds numbers of the present tests may lead to another effect - that of vorticity interaction. Several investigators (refs. 13-17) have studied convective heating in the vorticity-interaction regime. The effect of vorticity interaction on the present data was estimated according to the theories of different investigators, and the results are presented in the following table, where the ratio of convective heating rate with vorticity interaction to that without vorticity interaction is tabulated.

$\frac{\dot{q}_{vorticity}}{\dot{q}}$ / Velocity, ft/sec	References 14 and 16	References 13 and 15	Reference 17
24,000	None	None	None
36,000	1.01	1.08	Not available
41,000	1.02	1.09	1.18

No attempt was made to correct the data for vorticity interaction.

For the present tests radiative heating was always less than 1 percent of convective heating and was therefore neglected.

The degree of equilibrium attained in the shock layer and boundary layer is of interest in any heat-transfer test since it determines the possibility of catalytic surface-action effects on the measurements and is useful in assessing the applicability of the results to actual flight conditions. Applying the same methods used by Rose and Stankevics (ref. 8) in their treatment of this problem for shock-tube tests leads to the following statements for the present tests. First, it is probable that the shock layer has reached equilibrium both chemically and electronically at the edge of the boundary layer. The free-flight wind-tunnel measurements of air radiation on blunt models of Page and Arnold (ref. 18), scaled to the present model size, indicate that this is the case. Second, it is probable that the chemistry of the boundary layer is at least partially frozen, since the ratio of the diffusion time across the boundary layer to the recombination time for oxygen atoms (as defined in ref. 5) is 10^{-2} to 10^{-3}. At the lowest values of this ratio, reference 5 shows that for completely noncatalytic surfaces the reduction in heat transfer is 15 percent. Since it is probable that nickel and aluminum surfaces are catalytic, the heat-transfer measurements taken with these materials should be considered free of any significant reduction in heat transfer due to recombination of atoms. Third, it is difficult to estimate the state of ionization equilibrium in the boundary layer. Rose and Stankevics consider three mechanisms for ionic recombination, the fastest of which is collisional

radiative recombination and the slowest is electron three-body recombination. If collisional radiative recombination is the dominant process, then electronic equilibrium will be achieved in the boundary layer (ref. 8) and the catalytic activity of the surface with respect to recombination of ions and electrons cannot influence the heat transfer. On the other hand, if the electron three-body recombination process dominates, electronic equilibrium probably will not occur in the boundary layer (ref. 8) and surface catalytic activity may be important. Thus of the states considered, the electronic state of the boundary layer is the least certain. It can be concluded from the above remarks that catalytic surface activity is probably not a major influence in the present tests.

REFERENCES

1. Seiff, Alvin: A Progress Report on the Ames Hypervelocity Free-Flight Facilities and Some of the Current Research Problems Being Studied in Them. Presented at AIAA National Summer Meeting, Los Angeles, June 17-20, 1963. AIAA Paper 63-162.

2. Chapman, Gary T.; and Jackson, Charles T., Jr.: Measurement of the Heat Transfer to Bodies of Revolution in Free Flight by Use of a Catcher Calorimeter. NASA TN D-1890, 1963.

3. Carslaw, H. S.; and Jaeger, J. C.: Conduction of Heat in Solids. Second ed., Oxford, Clarendon Press, 1959.

4. Chapman, Dean R.: An Approximate Analytical Method for Studying Entry Into Planetary Atmospheres. NACA TN 4276, 1958.

5. Fay, J. A.; and Riddell, F. R.: Theory of Stagnation Point Heat Transfer in Dissociated Air. J. Aero. Sci., vol. 25, no. 2, Feb. 1958, pp. 73-85, 121.

6. Rose, P. H.; and Stark, W. I.: Stagnation Point Heat-Transfer Measurements in Dissociated Air. J. Aero. Sci., vol. 25, no. 2, Feb. 1958, pp. 86-97.

7. Gruszczynski, J. S.; and Warren, W. R., Jr.: Experimental Heat Transfer Studies of Hypervelocity Flight in Planetary Atmospheres. AIAA Paper 63-450.

8. Rose, P. H.; and Stankevics, J. O.: Stagnation Point Heat Transfer Measurements in Partially Ionized Air. Res. Rep. 143, Avco-Everett Res. Lab., April 1963.

9. Offenhartz, E.; Weisblatt, H.; and Flagg, R. F.: Stagnation Point Heat Transfer Measurements at Super Satellite Speeds. J. Roy. Aeron. Soc., vol. 66, no. 613, Jan. 1962, p. 53.

10. Nerem, R. M.: Measurements of Aerodynamic and Radiative Heating at Super-orbital Velocities. Ohio State Univ. Res. Found. Rep. 1598-1, 1964.

11. Collins, D. J.; and Spiegel, J. M.: Effect of Gage Material on Convective Heat Transfer. AIAA J., vol. 2, no. 4, April 1964, pp. 777-778.

12. Hoshizaki, H.: Heat Transfer in Planetary Atmospheres at Supersatellite Speeds. ARS J., vol. 32, 1962, pp. 1544-1551.

13. Ferri, Antonio; Zakkay, Victor; and Ting, Lu: Blunt-Body Heat Transfer at Hypersonic Speed and Low Reynolds Numbers. J. Aero. Sci., vol. 28, no. 12, Dec. 1961, pp. 962-971, 991.

14. Hayes, Wallace D.; and Probstein, Ronald F.: Hypersonic Flow Theory. Academic Press, Inc., N. Y., 1959, p. 372.

15. Cheng, H. K.: Hypersonic Shock-Layer Theory of the Stagnation Region at Low Reynolds Number. Proceedings of the 1961 Heat Transfer and Fluid Mechanics Institute, Stanford Univ. Press, Stanford, Calif., 1961, pp. 161-175.

16. Van Dyke, Milton: A Review and Extension of Second-Order Hypersonic Boundary-Layer Theory. Rarefied Gas Dynamics, vol. 2. Academic Press, Inc., New York, 1963, pp. 212-227.

17. Howe, John T.; and Sheaffer, Yvonne S.: Mass Addition in the Stagnation Region for Velocity up to 50,000 Feet Per Second. NASA TR R-207, 1964.

18. Page, William A.; and Arnold, James O.: Shock-Layer Radiation of Blunt Bodies at Reentry Velocities. NASA TR R-193, 1964.

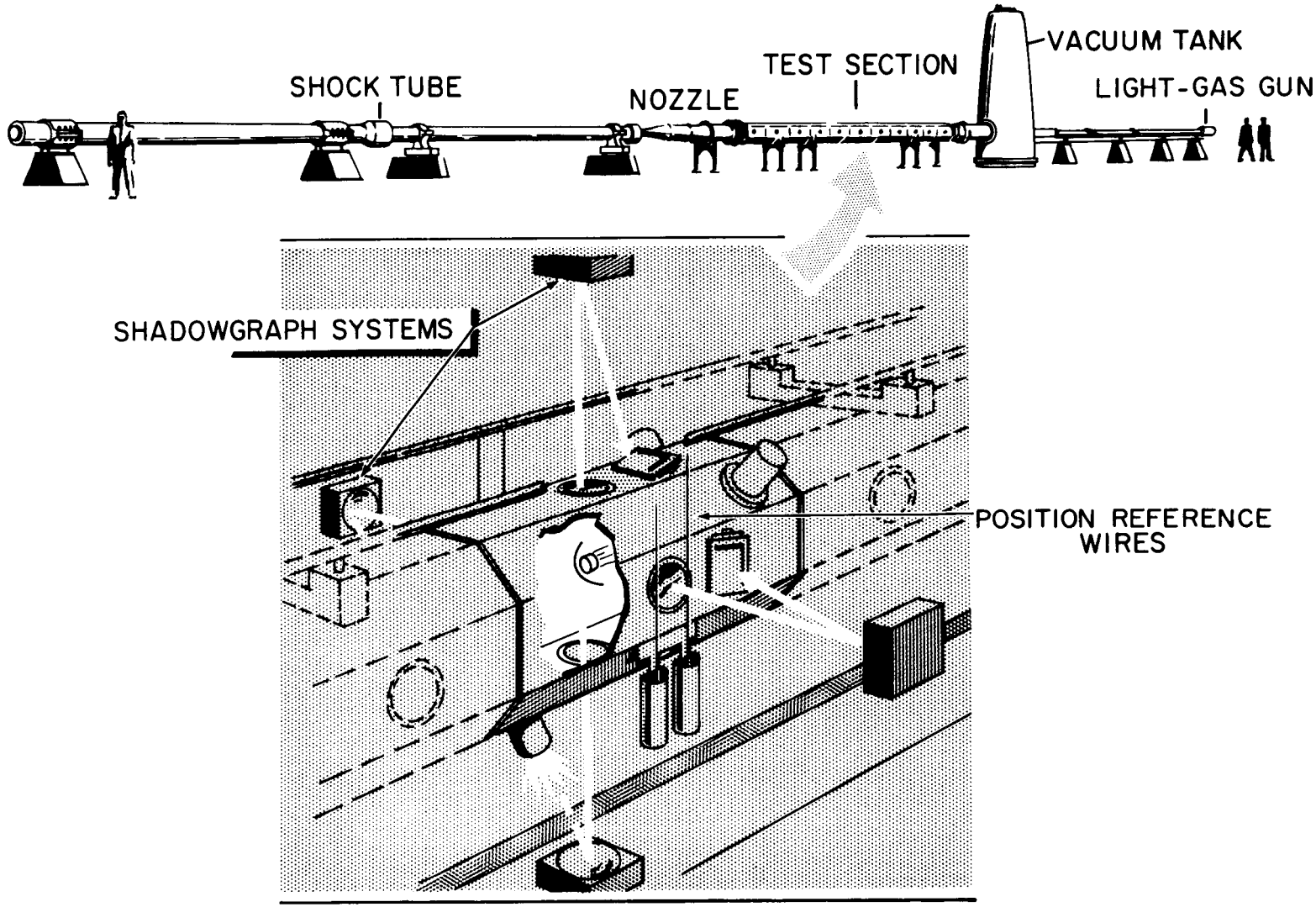

Figure 1.- Schematic drawing of Prototype Hypervelocity Free-Flight Facility.

A-32126-7

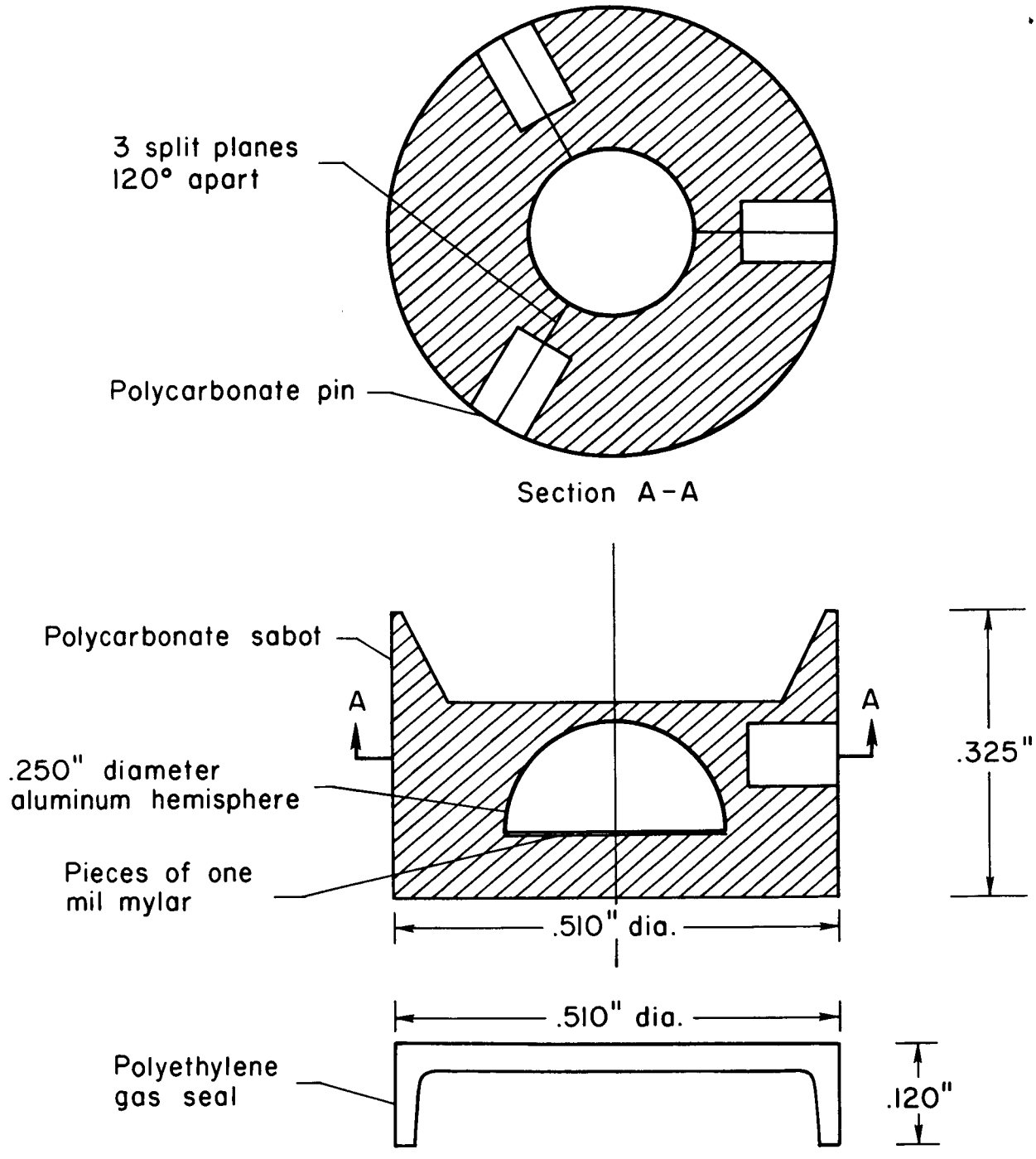

Figure 2.- Sketch of typical model, sabot, and gas seal.

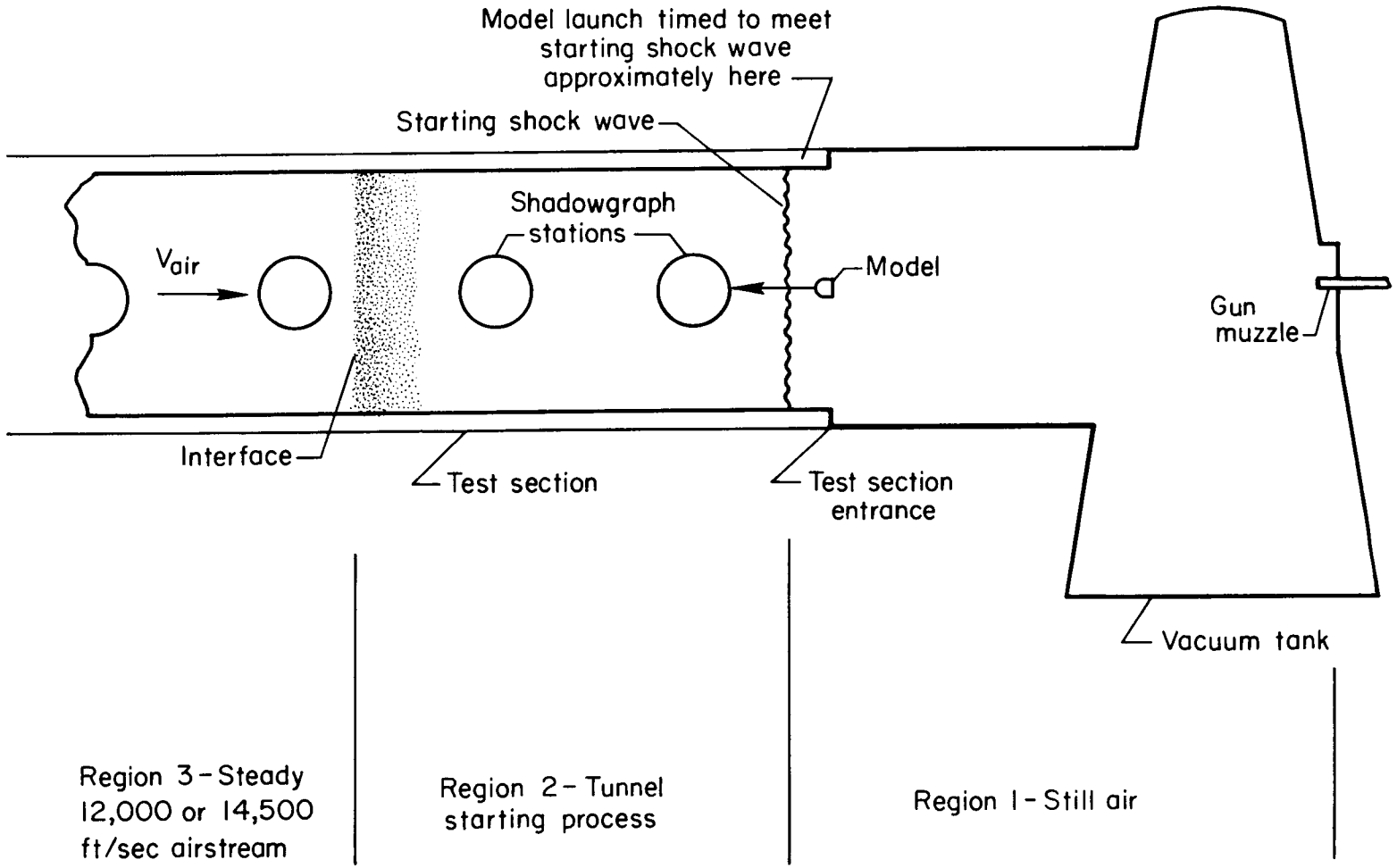

Figure 3.- Schematic for air-on operation. Not to scale.

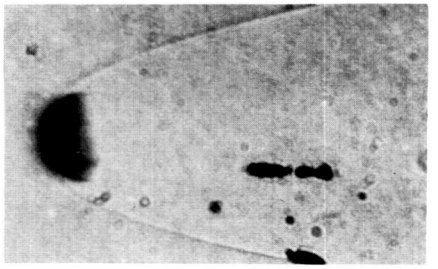

Station 1; t = 0.634 ms;
T_w = 1020° F

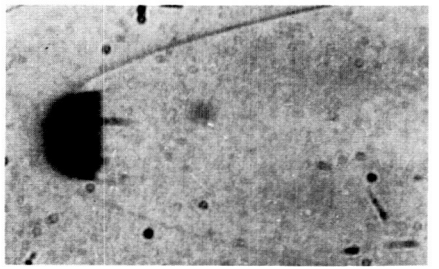

Station 2; t = 0.807 ms;
T_w = 1116° F

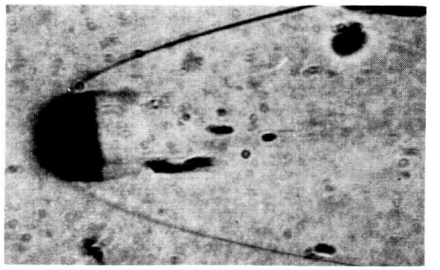

Station 3; t = 0.983 ms;
T_w = 1198° F

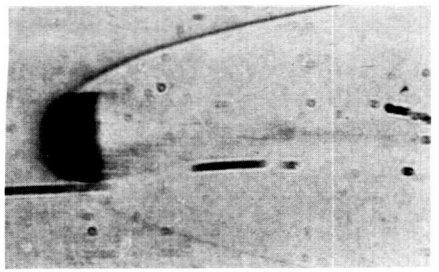

Station 4; t=1.161 ms;
T_w = 1267° F

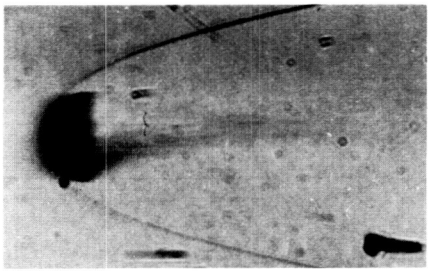

Station 5; t = 1.341 ms;
T_w = 1327° F

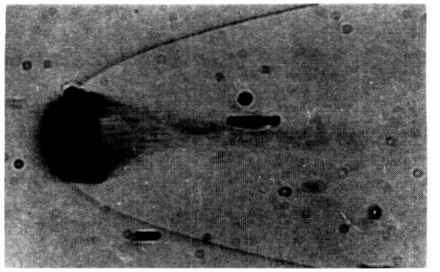

Station 6; t = 1.523 ms;
T_w = 1378° F

A-32126-8

Figure 4.- Shadowgraphs of melting onset for aluminum models. Aluminum (7075-T6) melting temperature = 1180° F, V_L = 24,200 ft/sec, P_∞ = 0.092 atm. Model is slightly blurred because of long (approximately 0.1 μsec) exposure time. Spots on pictures are imperfections in windows.

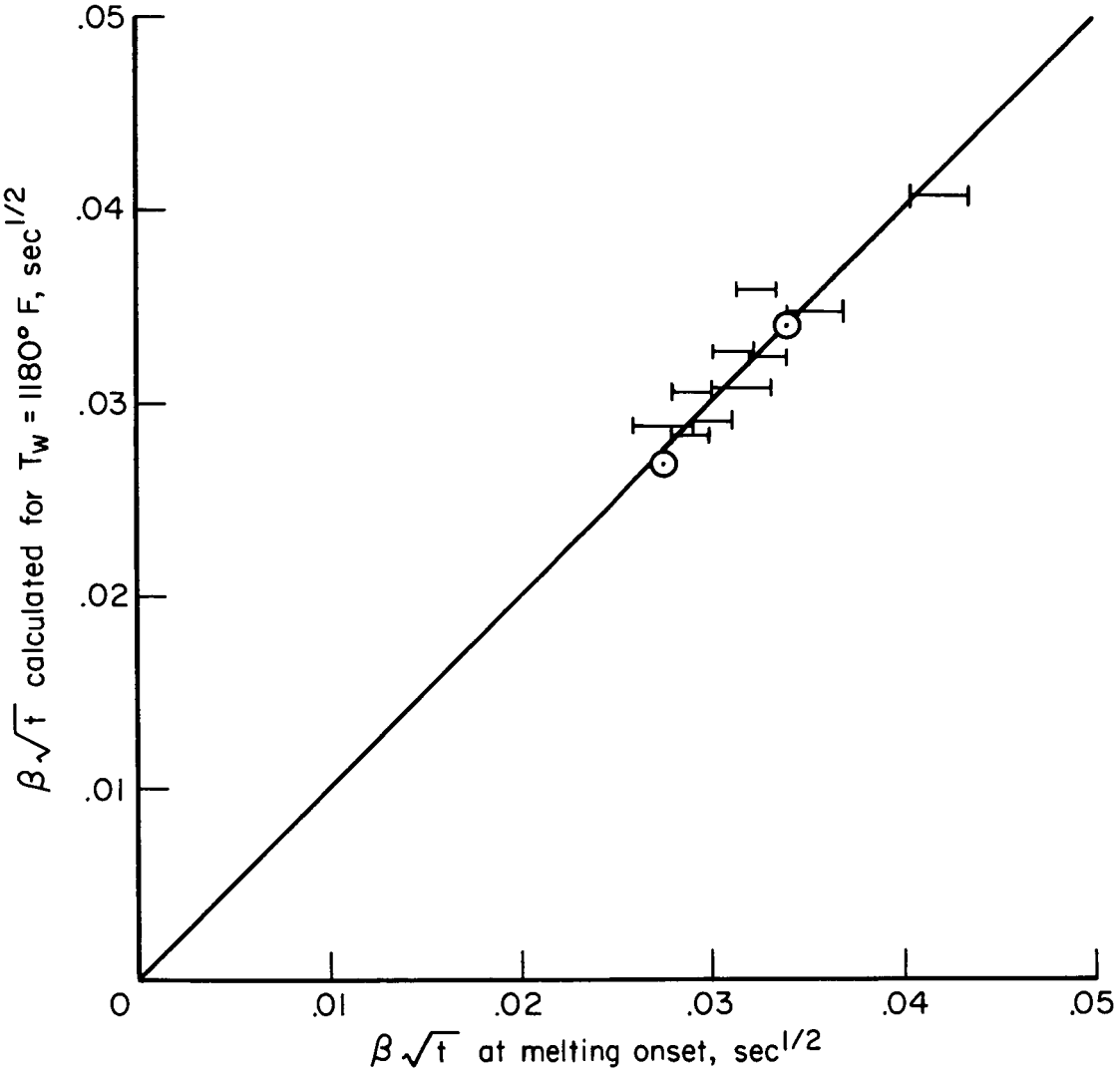

Figure 5.- Correlation plot for aluminum data; V = 24,000 ft/sec.

	T_w, °F (calculated)	
Station 1 t = 0.628 msec	1118	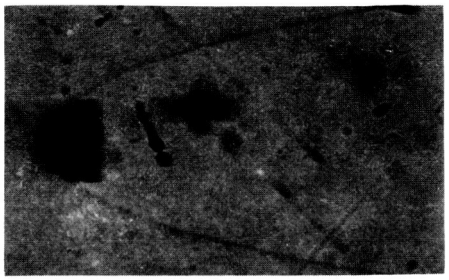
Station 2 t = 0.801 msec (Kerr cell shutter)	1224	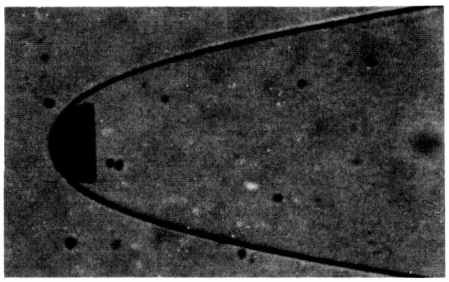
Station 3 t = 0.956 msec	1312	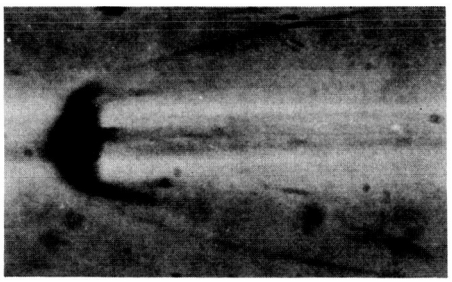
Station 4 t = 1.153 msec (Kerr cell shutter)	1386	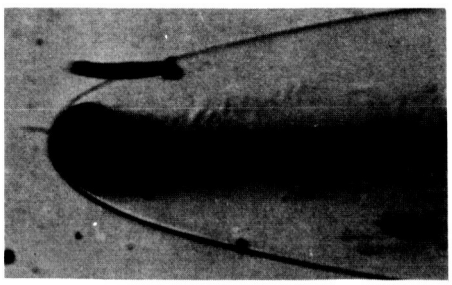

Figure 6.- Shadowgraphs of melting onset for nickel-plated aluminum models; V_L = 24,460 ft/sec, P_∞ = 0.105 atm.

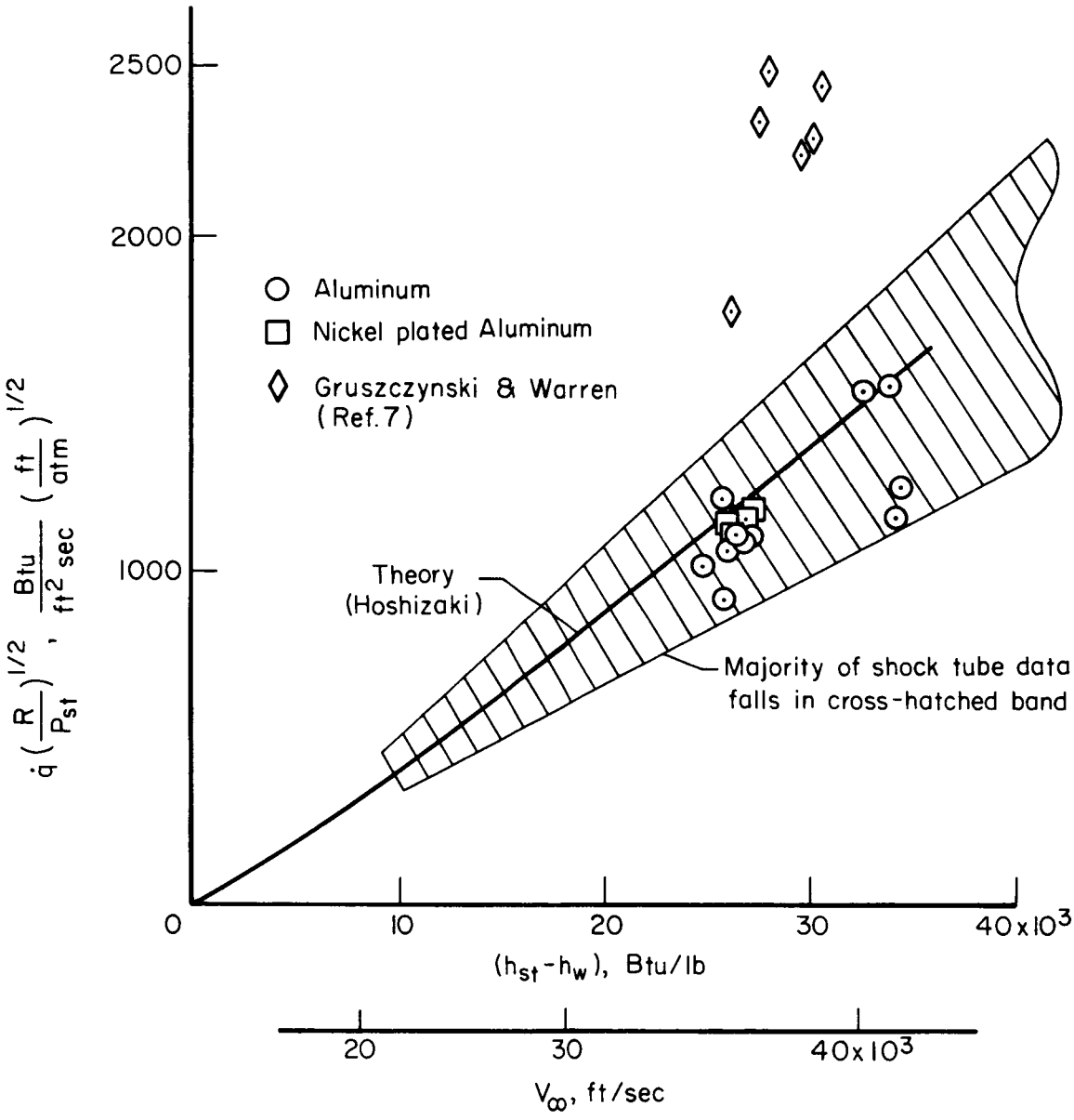

Figure 7.- Convective heating data.